

An Adaptive Fusion Estimation Algorithm for State of Charge of Lithium-ion Batteries Considering Wide Operating Temperature and Degradation

Xing Shu¹, Guang Li², Jiangwei Shen¹, Wensheng Yan¹, Zheng Chen^{1,2*} and Yonggang Liu^{3*}

¹Faculty of Transportation Engineering, Kunming University of Science and Technology, Kunming, 650500, China

²School of Engineering and Materials Science, Queen Mary University of London, London, E1 4NS, United Kingdom

³State Key Laboratory of Mechanical Transmissions & School of Automotive Engineering, Chongqing University, Chongqing, 400044, China

Email: shuxing92@163.com, g.li@qmul.ac.uk, shenjiangwei6@163.com, yanwensheng65@sina.com, chen@kust.edu.cn, andylyg@umich.edu

Corresponding Author: Zheng Chen (chen@kust.edu.cn) and Yonggang Liu (andylyg@umich.edu)

Abstract: In this paper, an adaptive fusion algorithm is proposed to robustly estimate the state of charge of lithium-ion batteries. An improved recursive least square algorithm with a forgetting factor is employed to identify parameters of the built equivalent circuit model, and the least square support vector machine algorithm is synchronously leveraged to estimate the battery state of health. On this basis, an adaptive H-infinity filter algorithm is applied to predict the battery state of charge and to cope with uncertainty of model errors and prior noise evaluation. The proposed algorithm is comprehensively validated within a full operational temperature range of battery and with different aging status. Experimental results reveal that the maximum absolute error of the fusion estimation algorithm is less than 1.2%, manifesting its effectiveness and stability when subject to internal capacity degradation of battery and operating temperature variation.

Key Words: adaptive H-infinity filter, least square support vector machine, model-based method, state of charge.

NOMENCLATURE

Abbreviations

EVs	electric vehicles	AUKF	adaptive unscented Kalman filter
BMS	battery management system	ASR-SPKF	adaptive square root sigma-point Kalman filter
SOC	state of charge	A-SPKF	adaptive sigma-point Kalman filter
SOH	state of health	RLS	recursive least square
SOP	state of power	AEKF	adaptive extended Kalman filter
SOE	state of energy	FF-RLS	recursive least square with forgetting factor
SOF	state of function	AHIF	adaptive H-infinity filter
OCV	open circuit voltage	LS-SVM	least squares support vector machine
ECM	equivalent circuit model	GA	genetic algorithm
PF	particle filter	RMSE	root-mean-square error
KF	Kalman filter	SVM	support vector machine

EKF	extended Kalman filter	RBF	radial basis kernel
CKF	cubature Kalman filter	CC	constant current
UKF	unscented Kalman filter	CC-CV	constant current–constant voltage
HIF	H-infinity filter	MSE	mean square error
DEKF	dual extend Kalman filter	UDDS	urban dynamometer driving schedule
RLS-EKF	recursive least square-extended Kalman filter	GA-AHIF	genetic algorithm based adaptive H-infinity filter
NC-EKF	noise compensation-extended Kalman filter	PI	proportional-integral
<i>Symbols</i>			
V_{OCV}	open circuit voltage	T	battery temperature
R_0	internal ohmic resistance	V_{test}	measurement voltage
R_1	polarization resistance	N	test time
C_1	polarization capacitance	u_k	input variable
E	terminal voltage	x_k	state variable
I	loading current	y_k	measurement variable with noise
V_0	ohmic voltage	z_k	linear combination of estimation states
V_1	polarization voltage	L_k	unit matrix
s_k	state of charge at sampling k	w_k	system noise
η	coulomb efficiency	v_k	measurement noise
Δt	sampling interval time	P_0	symmetric positive matrices
Q_n	battery rated capacity	Q_k	symmetric positive matrices
w_1	process noise for state of charge	R_k	symmetric positive matrices
w_2	process noise for polarization voltage	S_k	symmetric positive matrices
v	measurement noise	J	cost function for H-infinity filter
$G(s)$	transformation function	ε	user-specified boundary value
a_i	coefficients associated with the model parameters	ξ	deviation vector
Φ_k	input data matrix	C	weight of support vector machine
θ_k	parameter matrix	L	Lagrange function
K_{FF-RLS}	gain matrix of FF-RLS	α_i	Lagrange multiplier
$P_{FF-RLS,k}$	covariance matrix of FF-RLS	$K(x, x_i)$	kernel function
w	white noise information	V_{start}	starting recode voltage
λ	forgetting factor	V_{stop}	ending recode voltage
p_i	fitting coefficients of OCV		

I. INTRODUCTION

Transportation electrification can effectively mitigate environmental pollution and greenhouse gas emissions incurred by massive combustion of fossil fuels [1]. Electric vehicles (EVs), representing an important class of development direction, have attracted wide attention due to their zero emissions, high efficiency and superior driving performances [2]. Currently, most of EVs are equipped with lithium-ion batteries for storage of electric energy [3, 4]. To guarantee safe efficient operation of batteries, a serviceable battery management system (BMS) is indispensable [5]. The main task of BMS includes accurate measure of battery current, voltage and temperature and on this basis, estimation and evaluation of the inner status [6], i.e., state of X , where X can be charge (SOC) [7], health (SOH) [8, 9], power (SOP) [10], energy (SOE) and function (SOF) [11]. Amongst them, SOC refers to the ratio of remaining available capacity over the nominal capacity and directly correlates with current, temperature and terminal voltage of batteries. Its effective estimation is vital to supply the reference for estimation of remaining driving mileage and avoid abuse operation (over-charge/ discharge). Hence, the estimation algorithm needs to be accurate, quick convergent, reliable and robust [3], and is indeed a challenging task.

To now, a variety of advanced methods have been proposed, applied and validated to achieve SOC estimation. Typical ones include coulomb counting, open circuit voltage (OCV) based calibration, data driven and model-based algorithms [12]. The coulomb counting method estimates SOC by directly integrating the current flowing into and out of batteries over time. Obviously, it is simple and easy to implement in practice, and yet difficult to guarantee estimation accuracy, as it is easily disturbed by measurement error and noise of current, and particularly depends heavily on the initial SOC value [13]. The OCV-based method can obtain SOC accurately with the offline calibrated relationship between OCV and SOC. Apparently, it is not applicable for real-time application, since it is almost not possible to acquire the OCV online. The data driven based method directly extracts internal characteristics of batteries by means of a large amount of operation data, from which the nonlinear mapping relationship between SOC and feature variables is established. The above methods do not require deep understanding of battery operation and inner electrochemical reaction characteristics. However, the estimation accuracy depends largely on selection of feature parameters as well as quality and quantity of training data [14]. The model-based estimation methods are extensively accepted because of their high precision, noise elimination and independence of initial values. Additionally, they sufficiently merge external voltage, current and temperature information and refer to the offline calibration test and model establishment [7, 15]. To

apply model-based algorithms, it is necessary to characterize dynamic and static electrical performances of batteries. Consequently, popular manners, such as equivalent circuit model (ECM) [16], complex electrochemical model [17] and pseudo single particle model [18], are elaborated and applied. Presently, the most popular modeling manner when conducting SOC estimation belongs to the ECM, due to its acceptable precision and fast calculation speed. On this basis, typical filters are harnessed to improve the observation precision, including particle filter (PF) [19], Kalman filter (KF) and its extensions such as extend KF (EKF) [20], adaptive EKF (AEKF) [21], cubature KF (CKF) [22], and unscented KF (UKF) [23], nonlinear observer [24], and H-infinity filter (HIF) [25]. In [26], three SOC methods including the dual EKF (DEKF), recursive least square (RLS)-EKF (RLS-EKF) and noise compensation-EKF (NC-EKF) are systemically compared and evaluated. Numerical results manifest that the DEKF and NC-EKF are more robust than RLS-EKF when magnitude of noises aggravates, and the RLS-EKF and NC-EKF feature the least and highest computation intensity among these filters, respectively. In [27], an adaptive UKF (AUKF) is leveraged to estimate the SOC of battery modules grouped by cells in series connection. Compared with UKF and EKF, the experimental results reveal that the improved AUKF method can track the reference SOC and exhibit high robustness when the process and measurement statistics noises vary stochastically. In [28], an augmented battery model is divided into a SOC sub-model and a resistance-capacitance (RC) circuit sub-model to reduce the cross interference between SOC and the voltage of RC network. The experimental results demonstrate the efficacy of reducing SOC oscillation and decreasing estimation errors. In addition, electrochemical model and its reduced-order format (such as single particle model) are progressively exploited for SOC estimation. In [29], the EKF is adopted based on the single particle model to estimate the SOC. A more precise electrochemical model is developed in [30] considering the influence of electrical double layer structure, and the EKF observer is leveraged for SOC estimation. Ref. [31] employs the Padé approximation and third-order residual grouping methods to reduce the computational complexity of the original electrochemical model. Based on the reduced-order electrochemical model, the adaptive square root sigma-point Kalman filter (ASR-SPKF) is addressed to predict the battery SOC. The estimation results reveal that the ASR-SPKF can lead to better SOC prediction performance, compared with another two nonlinear filter algorithms, i.e., AEKF and adaptive sigma-point Kalman filter (A-SKF). In comparison with ECM, electrochemical models can characterize the battery's electrical performance and inner chemical reactions more precisely; however, the intensive calculation burden

hinders their online application potential. Instead, ECM is a proper candidate to balance the modeling precision and calculation complexity and is therefore still employed in this study.

In practice, batteries operate within a wide temperature range (usually $-20\text{ }^{\circ}\text{C}$ to $50\text{ }^{\circ}\text{C}$), and in this context, the model parameters of battery may change with temperature in a nonlinear manner. Similarly, performance degradation of batteries with cycling also leads to variations of model parameters. To address these variations, many efforts have been made to online update model parameters and to cope with external varying conditions and internal parameter variations [26]. In [32], a temperature compensated model is built, and the EKF is investigated to improve the estimation precision of SOC. Ref. [33] analyzes the relationship between the differential voltage (DV) and incremental capacity (IC) in a narrow scope and achieves the simultaneous online estimation of battery capacity and SOC. In [34], a joint algorithm incorporating RLS and AEKF is leveraged to identify the battery parameters and estimate the SOC simultaneously. In addition, the battery capacity is predicted by the Elman neural network in real-time operations. The numerical results highlight that the estimation error of SOC is less than 2% at room temperature with different aging status. Nonetheless, a wide operating temperature range is not explicitly taken into account, and the maximum estimation error can reach as high as 6% when the temperature is beyond the normal range. In [35], a Thevenin electric model integrating temperature compensation is introduced and the model parameters are identified by the RLS method under the conditions of different temperatures. In [25], a multi-scale dual HIF is proposed to estimate the battery SOC and capacity simultaneously. However, the operating temperature is not fully considered, and the estimation performance is not evaluated when the temperature varies.

As discussed above, even significant contributions have been made to improve SOC estimation accuracy in the whole operation range of battery, there still exists a certain room for further improvement when fully considering temperature variation and battery degradation. Motivated by this fact, an advanced fusion estimation algorithm for batteries is developed based on the ECM considering the whole operating temperature and capacity degradation. First, the battery parameters are identified by an improved RLS with a forgetting factor (FF-RLS) for adaption to environmental temperature variation and capacity degradation. On this basis, the battery SOC is estimated by the adaptive HIF (AHIF) algorithm to cope with the interference of system variation and measurement noise. Furthermore, the least square support vector machine (LS-SVM) is simultaneously employed to estimate the battery SOH, thus contributing to the estimation of SOC. The experimental results in terms of variation of capacity and operating temperature demonstrate that the algorithm outperforms other

commonly used model-based methods, such as AEKF. Moreover, the algorithm together with built ECM is still effective at low temperature and with degraded capacity. This is of great significance for SOC estimation when the battery ages.

The remainder of this paper is structured as follows. In Section II, the ECM and model parameter estimation for lithium-ion batteries are presented. Section III introduces the adaptive fusion algorithm for the SOC and SOH estimation. Section IV presents and discusses the validation results. Finally, the concluding remarks and future work are given in Section V.

II. LITHIUM-ION BATTERY MODEL AND PARAMETERS

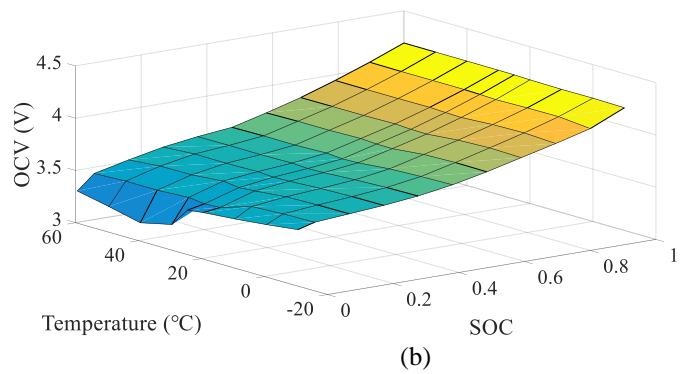
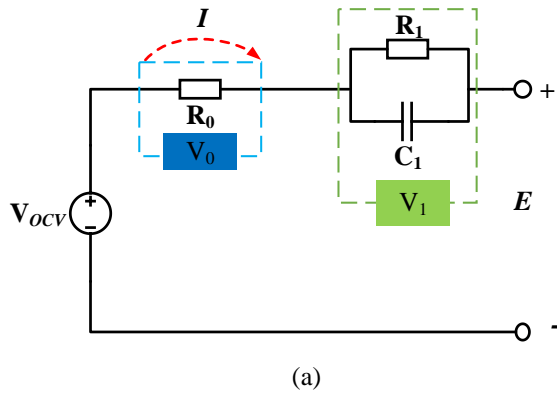
A. Lithium-ion Battery Cell Model

Three broad categories of battery models, including ECM, data driven model and electrochemical model, are widely employed to characterize the battery electrical performance. Among these models, the ECM can not only capture the battery's dynamic and static characteristics with preferable precision, but also feature low computation intensity, thereby enabling online real-time application [27]. Thus, the ECM, as depicted in Fig. 1 (a), is employed in this study to describe the electrical behavior of battery. The SOC is expressed as the percentage of remaining capacity over the rated discharging capacity, as:

$$s_{k+1} = s_k - \eta I_k \Delta t / Q_n \quad (1)$$

where s_k represents the battery SOC at the sampling time k ; η denotes the coulomb efficiency; Δt represents the sampling time (unit: second), and Q_n is the battery rated capacity with the unit of Ampere-hour.

In this study, the target batteries are 21700 LiNMC cells and the detailed specifications are listed in Table I.



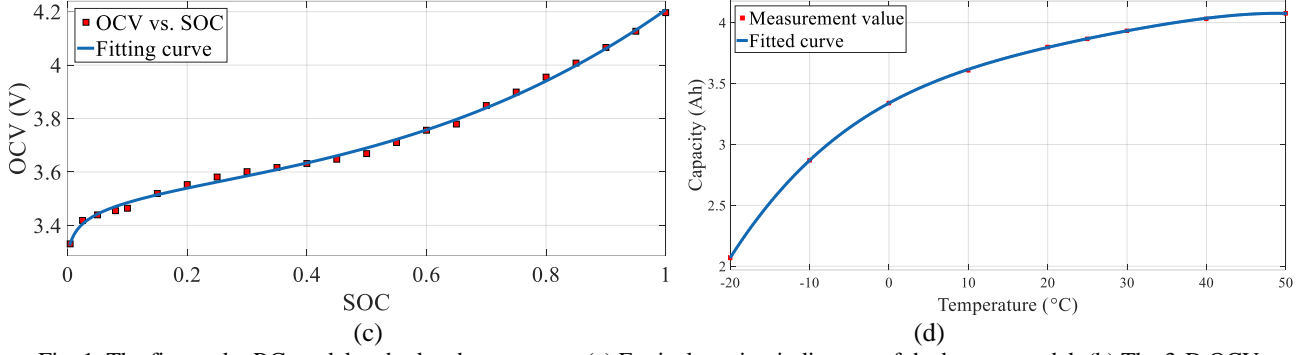


Fig. 1. The first-order RC model and related parameters. (a) Equivalent circuit diagram of the battery model; (b) The 3-D OCV response surface; (c) The SOC-OCV correlation and fitting results; (d) The Initial capacity at different temperatures.

Table I Specification of the test battery

Items	Specification
Cathode material	Li(NiCoMn)O ₂
Anode material	Graphite
Nominal capacity	4 Ah
Allowed operating range of voltage	2.75-4.2 V
Rated voltage	3.65 V
Allowed charging temperature	0-45 °C
Allowed discharging temperature	-20-60 °C

According to Fig. 1 (a), the following equations can be formulated, as:

$$\begin{cases} \dot{s} = -\frac{1}{Q_n} I_t + w_1 \\ \dot{V}_1 = -\frac{1}{R_1 C_1} V_1 + \frac{1}{C_1} I_t + w_2 \end{cases} \quad (2)$$

$$E = V_{oc}(s, T) - V_1 - R_0 I_t + v \quad (3)$$

where V_{ocv} denotes the ideal OCV, R_0 is the internal ohmic resistance, R_1 and C_1 are respectively the polarization resistance and capacitance, E is the terminal voltage, and I denotes the loading current. V_0 and V_1 represent the ohmic voltage and polarization voltage across R_0 and R_1 ; v represents the measurement noise; and w_1 and w_2 denote the process noise for SOC and V_1 , respectively.

B. Parameters Acquisition

Given the strong nonlinear time-varying characteristics of batteries, it is imperative to construct an online parameter identification algorithm for sufficiently responding to the battery's electrical performance. Additionally, the offline identification algorithm is also beneficial to quantitatively describe the relationship between OCV and SOC, temperature and initial capacity. To attain it, the genetic algorithm (GA) is employed to achieve the offline identification.

1). Online Identification

According to (2), the state space equation of battery model can be discretized as:

$$\begin{cases} V_{1,k} = e^{-\frac{\Delta t}{R_1 C_1}} V_{1,k-1} + (1 - e^{-\frac{\Delta t}{R_1 C_1}}) R_1 I_{k-1} \\ E_k = V_{oc,k} - V_{1,k} - R_0 I_k \end{cases} \quad (4)$$

where E_k , $V_{1,k}$ and $V_{OCV,k}$ respectively denote the terminal voltage, polarization voltage and OCV at the k th sampling time, and I_k is the current at the k th sampling time. From (4), we can get:

$$E_k = V_{OCV,k} - \left(e^{-\frac{\Delta t}{R_1 C_1}} V_{1,k} + (1 - e^{-\frac{\Delta t}{R_1 C_1}}) R_1 I_{k-1} \right) - I_k R_0 \quad (5)$$

By eliminating $V_{1,k}$, we can attain:

$$E_k - V_{OCV,k} = e^{-\frac{\Delta t}{R_1 C_1}} (E_{k-1} - V_{OCV,k-1}) + (-R_0) I_k + \left(e^{-\frac{\Delta t}{R_1 C_1}} R_0 - (1 - e^{-\frac{\Delta t}{R_1 C_1}}) R_1 \right) I_k \quad (6)$$

Here, we assume that the OCV at the k th step $V_{OCV,k}$ is equal to $V_{OCV,k-1}$ at the $(k-1)$ th step. Then, the discretization calculation can be rewritten as:

$$E_k = a_1 + a_2 E_{k-1} + a_3 I_k + a_4 I_{k-1} \quad (7)$$

where a_i ($i=1,2,3,4$) express the coefficients. Consequently, we can attain:

$$\begin{cases} y_k = \Phi_k \theta_k + w \\ \Phi_k = [1 \quad E_{k-1} \quad I_k \quad I_{k-1}] \\ \theta_k = [a_1 \quad a_2 \quad a_3 \quad a_4]^T \\ y_k = E_k \end{cases} \quad (8)$$

where w denotes the white noise from the measurement, and

$$\begin{cases} a_1 = (1 - a_2) V_{OCV} \\ a_2 = e^{-\Delta t / (R_1 C_1)} \\ a_3 = -R_0 \\ a_4 = e^{-\Delta t / (R_1 C_1)} R_0 - (1 - e^{-\Delta t / (R_1 C_1)}) R_1 \end{cases} \quad (9)$$

From (9), the ECM parameters can be obtained, as:

$$\begin{cases} R_0 = -a_3 \\ R_1 = \frac{a_2 a_3 + a_4}{a_2 - 1} \\ C_1 = \frac{(1 - a_2) \Delta t}{(a_2 a_3 + a_4) \log(a_2)} \\ V_{OCV} = \frac{a_1}{1 - a_2} \end{cases} \quad (10)$$

As mentioned above, the battery model parameters can be easily influenced by the uncertain operation environment. The RLS algorithm based on adaptive filtering can compensate uncertainty of model parameters through recursive parameter correction, so as to accurately capture real-time characteristics of the system. However, for heuristic systems with slow continuous changes, the traditional RLS algorithm is difficult to track variation and provide reliable estimation results [36]. To tackle this issue, the FF-RLS is proposed to realize reliable estimation of model parameters [37]. The main solution steps of FF-RLS are summarized as follows:

1) Input data matrix and initialize parameter matrix

$$\begin{cases} \Phi_k = [1 & E_{k-1} & I_k & I_{k-1}] \\ \theta_0 = [a_{1_0} & a_{2_0} & a_{3_0} & a_{4_0}]^T \end{cases} \quad (11)$$

2) Determine the gain matrix and the covariance matrix

$$\begin{cases} K_{FF-RLS, k} = \frac{P_{FF-RLS, k-1} \Phi_k^T}{\lambda + \Phi_k P_{FF-RLS, k-1} \Phi_k^T} \\ P_{FF-RLS, k} = \frac{P_{FF-RLS, k-1} - K_{FF-RLS, k} \Phi_k P_{FF-RLS, k-1}}{\lambda} \end{cases} \quad (12)$$

where λ denotes the forgetting factor, and its function is to strengthen the role of new data and gradually weaken the function of old data. Usually, λ is set within [0.95, 1]. When λ equals 1, the algorithm degenerates to the conventional RLS.

3) Update the estimation parameters, as:

$$\hat{\theta}_k = \hat{\theta}_{k-1} + K_{FF-RLS} (y_k - \Phi_k \hat{\theta}_{k-1}) \quad (13)$$

4) $k = k + 1$ and go to step 1).

It is worth noting that although the FF-RLS can identify the battery parameters under the condition of rapid current excitation, unchanged or tiny varying current excitation still affect precision of parameter identification [38]. However, in practice, long time rest and constant current (CC) charging are inevitable. Thus, the current profiles need to be sufficiently diverse to achieve the battery extreme performance. As such, additional iteration process is designed in this paper to solve this problem. In the case of low current or CC, the FF-RLS is temporarily terminated and new parameters are obtained through the weighted average of historical model parameters. The iterative process is designed as:

$$\hat{\theta}_{k, average} = (1 - \frac{1}{\delta}) \hat{\theta}_{k-1, average} + \hat{\theta}_k \frac{1}{\delta} \quad (14)$$

where $\delta = (1 - \lambda^k)/(1 - \lambda)$. By adding a parameter update loop, the parameter identification method can be applied in any cycle experiment.

2). Offline Identification

To acquire the temperature-SOC-OCV model, a group of cells are tested at different operating temperatures with the specially designed current excitation. The experiment temperature is set to -20 °C to 50 °C with an interval of 10 °C. During the experiment, the voltage, current and temperature are recorded, and the sampling frequency is set to 1 Hz. All the cells are charged and discharged with the currents of 6 A (1.5C, where C denotes the rated capacity of battery with the unit of Ampere-hour) and 8 A (2C). The extracted OCV map at different temperatures and SOC values is depicted in Fig. 1 (b). It can be found that the OCV at different temperatures is not obvious when the SOC is greater than 20%. Here, by referring to the polynomial electrochemical equation introduced in [37], the relationship between OCV and SOC is formulated in (15), and the resulting curve at room temperature is plotted in Fig. 1 (c).

$$f_{ocv} = p_0 + p_1s + p_2s^2 + p_3s^3 + p_4/s + p_5 \ln(s) + p_6 \ln(1-s) \quad (15)$$

where p_i ($i=0,1,\dots,6$) are fitting coefficients. The battery initial maximum discharging capacity under different temperatures is plotted in Fig. 1 (d), and the relationship between maximum discharging capacity and temperature can be fitted as:

$$Q_n(T) = -1.681 \times 10^{-07} \cdot T^4 + 1.877 \times 10^{-05} \cdot T^3 - 0.0009316 \cdot T^2 + 0.03541 \cdot T + 3.338 \quad (16)$$

where T denotes the battery temperature. To further evaluate the performance of proposed online identification method, the commonly employed offline parameter identification method, i.e., GA, is applied to identify other parameters, including the ohmic resistance, polarization resistance and polarization capacitor [21, 39-41]. The root-mean-square error (RMSE) between the model output and measured voltage is selected as the fitness function:

$$RMSE = \sqrt{\frac{1}{N} \sum_{i=1}^N (E - V_{test})^2} \quad (17)$$

where V_{test} denotes the measurement voltage, and N represents the test time.

III. SOC AND SOH ESTIMATION

In this study, the joint estimation includes the SOC and SOH, both of which are strongly coupled, and precise SOC estimation relies on accurate SOH value.

A. The SOC Estimation Algorithm

The KF method assumes that the statistical characteristics of noise are known in advance [23]; however, it is difficult to obtain variance of noise in practice. In addition, the model errors incurred during the modeling process also deteriorate the estimation accuracy. To circumvent limitation of KF and uncertainty of model error and improve the robustness of estimation, the HIF algorithm is employed to estimate the battery SOC. We apply a standard linear time-varying discrete system, as:

$$\begin{cases} x_{k+1} = F_k x_k + w_k \\ y_k = H_k x_k + v_k \\ z_k = L_k x_k \end{cases} \quad (18)$$

where x_k is the state variable, y_k is measurement variable with noise, and z_k represents the linear combination of estimation states. L_k is a user-specified matrix, which is set to unit matrix in this paper; and w_k and v_k denote the system noise and measurement noise, respectively. The cost function of the HIF is defined as:

$$J = \frac{\sum_{k=0}^{N-1} \|z_k - \hat{z}_k\|}{\|x_0 - \hat{x}_0\|_{P_0}^2 + \sum_{k=0}^{N-1} (\|w_k\|_{Q_k}^2 + \|v_k\|_{R_k}^2)} \quad (19)$$

where P_0 , Q_k , R_k and S_k are positive definite matrices. Intuitively, it is difficult to minimize J , and for ease of finding its minimum value, a boundary condition is imposed to assist search of the suboptimal value, as:

$$J < \varepsilon \quad (20)$$

where ε denotes the user-specified boundary value. By incorporating (19) and (20), the boundary condition can be rewritten as:

$$J = -\varepsilon \|x_0 - \hat{x}_0\|_{P_0}^2 + \sum_{k=0}^{N-1} (\|w_k\|_{Q_k}^2 + \|v_k\|_{R_k}^2) - \varepsilon \sum_{k=0}^{N-1} \|z_k - \hat{z}_k\| < 0 \quad (21)$$

From the above discussion, we can find that the HIF can limit the noise interference to the H-infinity norm of the state estimation error within a restricted interference range. According to the first-order ECM, the input variable and state variable are defined as:

$$\begin{cases} u_k = I_k \\ x_k = [s_k, V_{1,k}]^T \end{cases} \quad (22)$$

Then, the state space equation of system can be expressed as:

$$\begin{cases} F_k = A_k x_k + B_k u_k \\ y_k = V_{oc,k} - V_{1,k} - R_0 u_k \end{cases} \quad (23)$$

where

$$A_k = \begin{bmatrix} 1 & 0 \\ 0 & e^{-\frac{\Delta t}{R_1 C_1}} \end{bmatrix}, B_k = \begin{bmatrix} \frac{\eta \Delta t}{Q_n} & \left(1 - e^{-\frac{\Delta t}{R_1 C_1}}\right) R_{1,k} \end{bmatrix}^T \quad (24)$$

Similar to the AEKF algorithm [21], the adaptive covariance calculation algorithm is added to the traditional HIF algorithm for updating the noise covariance matrix in the iterative process. Now, the general process of AHIF is illustrated in Table II.

From the implementation process of FF-RLS and AHIF, we can find that all the remaining parameters of the state space model, except the battery capacity Q_n , can be updated periodically. To attain estimation of Q_n , the support vector machine (SVM) is employed in this study.

Table II Algorithm of AHIF

Initialization	$\hat{x}_0^+ = E(x_0), P_0^+ = E[(x_0 - \hat{x}_0^+)(x_0 - \hat{x}_0^+)^T]$	(25)
Prior estimate of state	$\hat{x}_k^- = F_{k-1} \hat{x}_{k-1}^+$	(26)
Prior estimate of error covariance	$P_k^- = F_{k-1} P_{k-1}^+ F_{k-1}^T + Q_{k-1}$	(27)
Symmetric positive definite matrices update	$\bar{S}_k = L_k^T S_k L_k$	(28)
Condition judgment	$(P_k^-)^{-1} - \theta \bar{S}_k + H_k^T R_k^{-1} H_k > 0$	(29)
Innovation update	$e_k = y_k - H_k \hat{x}_k^-$	(30)
Adaptive estimation of measurement noise matrix	$\hat{M}_k = \frac{1}{N} \sum_{i=k-N+1}^k e_i e_i^T, \hat{R}_k = \hat{M}_k - H_k P_k^- H_k^T$	(31)
Gain matrix update	$K_k = F_k P_k^- (I - \theta \bar{S}_k P_k^- + H_k^T R_k^{-1} H_k P_k^-)^{-1} H_k^T R_k^{-1}$	(32)
Adaptive estimation of process noise matrix	$\hat{Q}_k = K_k \hat{M}_k K_k^T$	(33)
Measurement update of state estimate	$\hat{x}_k^+ = \hat{x}_k^- + K_k e_k$	(34)
Measurement update of error covariance	$P_k^+ = P_k^- (I - \theta \bar{S}_k P_k^- + H_k^T R_k^{-1} H_k P_k^-)^{-1}$	(35)

B. The SOH Estimation Algorithm

By comparing with other data driven algorithms, the SVM algorithm does not fall into the local extreme problem, and particularly it can be justified by rigorous mathematical proof. However, the general SVM shows complex solution process and intensive computation burden. The LS-SVM method is consequently developed

to solve the nonlinear regression estimation problem with less computation load and is proved suitable for battery SOH estimation [42-44]. To attain it, the following target function is established, as:

$$\min J(\mathbf{w}, \boldsymbol{\xi}) = \frac{1}{2} \mathbf{w}^T \mathbf{w} + \frac{C}{2} \sum_{i=1}^l \xi_i^2 \quad (36)$$

where $\boldsymbol{\xi} = [\xi_1 \ \xi_2 \ \dots \ \xi_l]$ is the deviation vector, and C denotes the weight, which can be identified to find the optimal hyper plane. In addition, the following constraint needs to be satisfied:

$$y_i [\mathbf{w}^T \boldsymbol{\varphi}(\mathbf{x}_i) + b] = 1 - \xi_i, i = 1, 2, \dots, l \quad (37)$$

The physical meaning of ξ_i in (37) can be explained as follows. When the sample \mathbf{x}_i lies outside the two critical hyperplanes, ξ_i is less than zero and it indicates the negative distance from \mathbf{x}_i to the nearest critical hyper plane. On the contrary, when \mathbf{x}_i is located between two critical hyperplanes, ξ_i is greater than zero; highlighting the positive distance from \mathbf{x}_i to the nearest critical hyper plane. The Lagrange function, as shown in (38), is defined and the maximum condition of the function is solved to achieve the minimization.

$$L(\mathbf{w}, \boldsymbol{\beta}, \boldsymbol{\xi}, \boldsymbol{\alpha}, C) = J(\mathbf{w}, \boldsymbol{\xi}) - \sum_{i=1}^l \alpha_i (\mathbf{w}^T \cdot \Phi(\mathbf{x}_i) + b + \xi_i - y_i) \quad (38)$$

where α_i represents the Lagrange multiplier. The optimization condition can be summarized as:

$$\frac{\partial L}{\partial \mathbf{w}} = 0, \quad \frac{\partial L}{\partial \boldsymbol{\alpha}} = 0, \quad \frac{\partial L}{\partial b} = 0, \quad \frac{\partial L}{\partial \boldsymbol{\xi}} = 0 \quad (39)$$

Given the above conditions, the following equations can be derived:

$$\begin{cases} \mathbf{w} = \sum_{i=1}^l \alpha_i \Phi(\mathbf{x}_i) \\ \mathbf{w} \cdot \Phi(\mathbf{x}_i) + b + \xi_i - y_i = 0 \\ \sum_{i=1}^l \alpha_i = 0 \\ \alpha_i = C \xi_i \end{cases} \quad (40)$$

By solving (40), the solution can be obtained:

$$f(x) = \sum_{i=1}^l \alpha_i K(\mathbf{x}, \mathbf{x}_i) + b \quad (41)$$

where $K(\mathbf{x}, \mathbf{x}_i)$ denotes the kernel function, and $K(\mathbf{x}, \mathbf{x}_i) = \Phi(\mathbf{x}_i)^T \Phi(\mathbf{x}_i)$. There are various types of kernel functions employed to solve the classification problem, such as Sigmoid kernel function, polynomial kernel function, radial basis kernel function (RBF), linear kernel function and Fourier kernel function [45]. Among

these kernel functions, the RBF kernel function can map the sample nonlinearly to a higher dimensional space with less numerical burden. Therefore, we selected it as the kernel function in this study, as:

$$K(\mathbf{x}, \mathbf{x}_i) = \exp\left(-\frac{\|\mathbf{x} - \mathbf{x}_i\|^2}{2\gamma^2}\right) \quad (42)$$

where γ denotes the width of RBF. Actually, the selection of feature variables plays a critical role in improving learning performance. For SOH estimation, the selected characteristics reflect the capacity variation of different cycle numbers [46], and Ref. [47] pointed out that the charging duration of CC stage decreases with degradation. In this study, the battery charging voltage profiles with different SOH levels are depicted in Fig. 2, and it can be observed that the CC stage obviously becomes shorter when the battery ages and the time interval of equal charging voltage difference gradually decreases. Hence, an appropriate feature variable from the CC charging voltage can be extracted to estimate the battery SOH. In this study, the charging duration $[V_{start} \ V_{stop}]$ is selected as the characteristic variable, where V_{start} and V_{stop} denote the starting and ending voltage value, respectively.

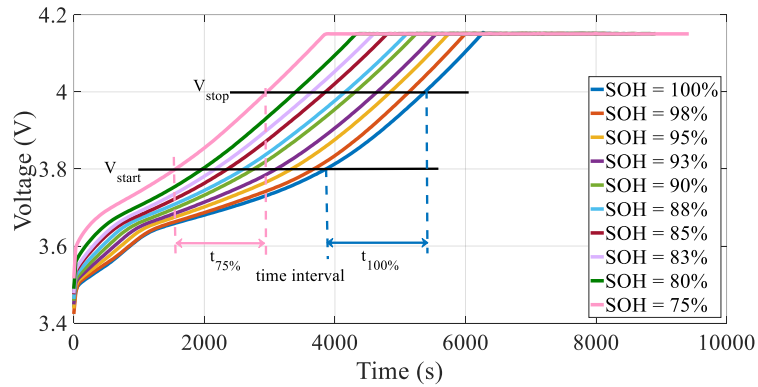


Fig. 2. Charging voltage profiles under different SOH.

C. Fusion Algorithm

On the basis of SOH estimation, the adaptive fusion algorithm based on AHIF is constructed to achieve the SOC estimation, as shown in Fig. 3. As can be seen, the fusion algorithm is divided into five parts: measurement, decision, parameters identification, SOH estimation and SOC estimation. When the battery operates, the measurement module monitors and records the battery current and terminal voltage. Then, the battery parameters are identified by the parameter identification module according to the measurement. When the decision module determines that the battery is in the CC charge stage, the SOH estimation module is activated to estimate the SOH, thus adaptively updating the battery capacity value. Finally, the SOC estimation module conducts the estimation by the AHIF algorithm with the updated model parameters and capacity.

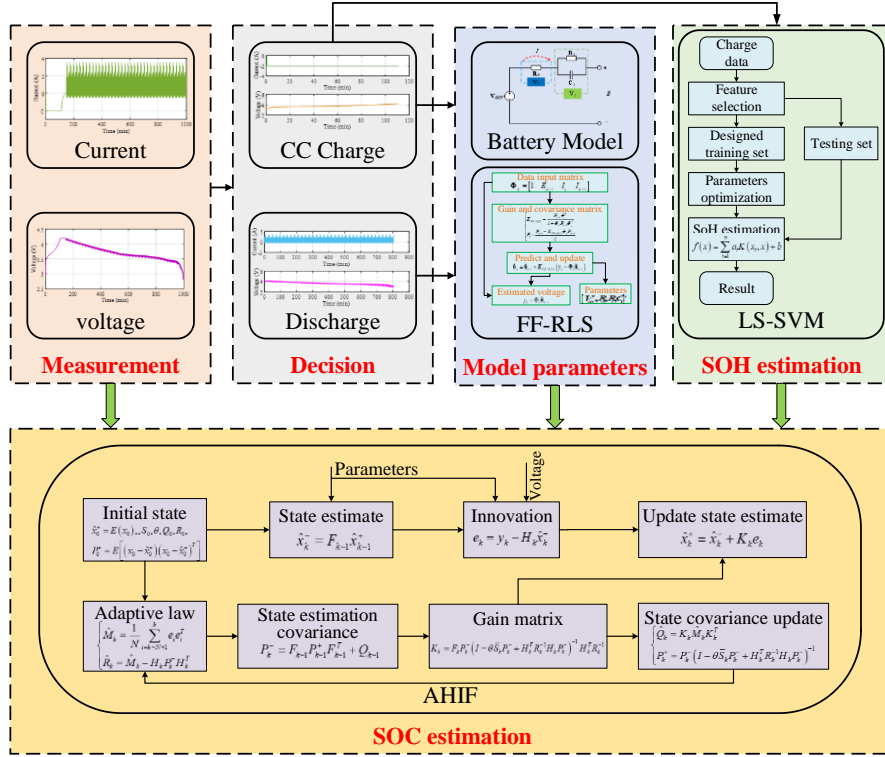


Fig. 3. Flowchart of the adaptive fusion algorithm.

According to the above estimation procedures, the model parameters, including ohmic resistance, polarization resistance, polarization capacity, OCV and battery capacity, can be timely updated. Thus, we can say that the battery SOC can be accurately estimated all the time, independent of the battery operating conditions. The detailed validation and discussion will be illustrated in the next section.

IV. EXPERIMENTAL VALIDATION AND DISCUSSION

To estimate the SOC, a preliminary task is that the algorithm needs to know the battery capacity value. Hence, in this section, the SOH estimation and validation is conducted first, followed by the SOC estimation. Note that the experimental results described in this study are derived from offline testing on a test platform, which consists a battery test system Arbin BT2000, a thermal controlled chamber, a host computer, and several test cells. The battery test device is responsible for charging/discharging the batteries according to the test plan and transmitting data to the host computer via the TCP/IP protocol. The programmable thermal chamber is applied to regulate the environment temperature. The host computer is used to store data and monitor battery operating state. The estimation algorithm is validated in Microautobox II, a product of dSPACE GmbH, of which the program is coded according to the simulation program built in MATLAB/Simulink on a laptop computer.

A. SOH Validation

First, a series of experiments are conducted to acquire enough data for training and validating the LS-SVM model. During the aging test, a constant current–constant voltage (CC-CV) charging strategy with the current of 0.5C is implemented in the charging process. When the terminal voltage reaches 4.15 V, the CV mode is activated until the current decreases to 0.02C. After shelving for 5 minutes, the cells are discharged with the current of 1C, and the cut-off voltage of CC discharge is 3 V. The whole test dataset is divided into three segments, wherein the dataset of cell 1 is divided into two parts with one for training and the other for verification; and the dataset of cell 2 is used to validate the model. According to the SOH estimation algorithm addressed previously, the feature voltage range is set from 3.58 V to 4.15 V. The SOH estimation results, the referred values and their difference are depicted in Fig. 4 and the evaluation criteria, including the mean absolute error, maximum absolute error, mean square error (MSE) and RMSE, are quantified in Table III. It can be found that the mean absolute error, maximum absolute error, MSE and RMSE are respectively 0.37%, 1.86%, 2.28×10^{-5} and 0.48%, justifying the feasibility of proposed algorithm. In addition, a raw dataset of another cell, namely cell 2, is applied to validate the performance of the training model. Fig. 4 (c) and (d) depict the estimation results. Although the estimation error of cell 2 is higher than the calibrated value, most of the maximum absolute error are still less than 2% (except several isolated points). Furthermore, the RMSE of two cells is restricted within 1%, highlighting the preferable performance of proposed estimation algorithm for SOH.

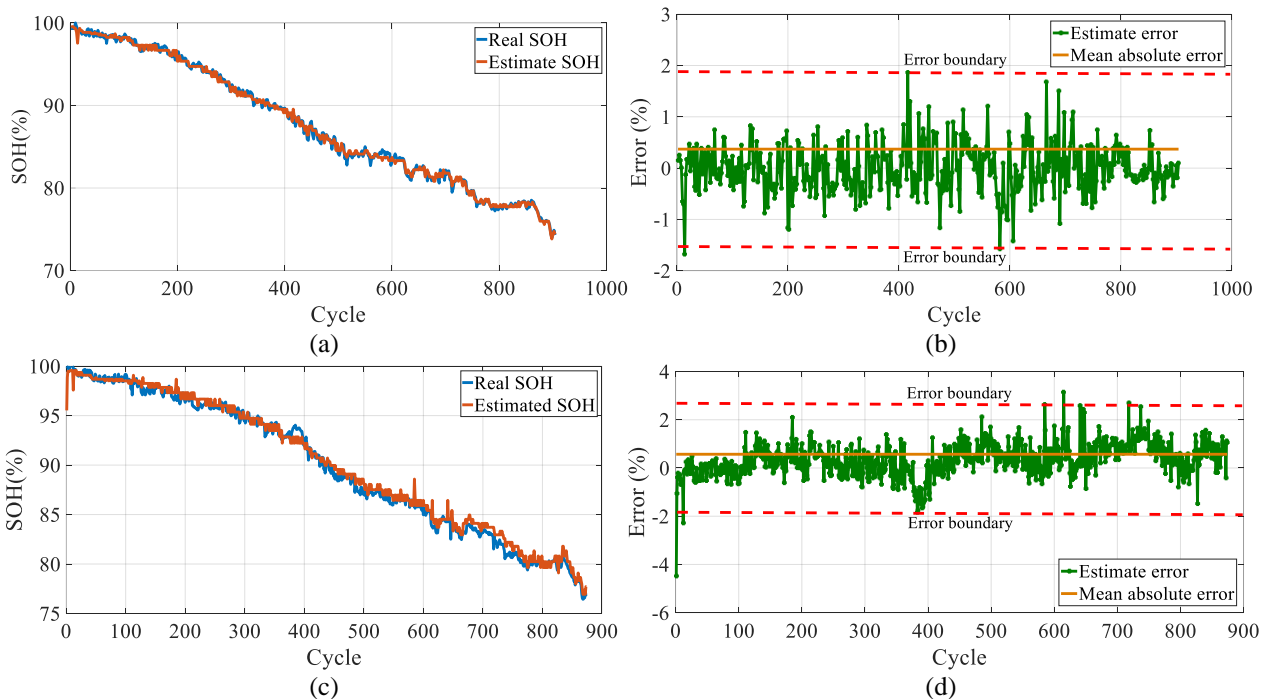


Fig. 4. SOH estimation results of two cells. (a) Measured and estimated SOH for cell 1; (b) Estimation error for cell 1; (c) Measured and estimated SOH for cell 2; (d) Estimation error for cell 2.

Table III. Estimation results of multiple battery experiments.

Cell number	Mean absolute error (%)	Maximum absolute error (%)	MSE	RMSE (%)
Cell 1	0.37	1.86	$2.28e^{-05}$	0.48
Cell 2	0.58	4.03	$5.61e^{-05}$	0.75

B. Comparison of SOC Estimation with Different Algorithms

To evaluate the SOC estimation performance, three commonly used methods are employed including the EKF, AEKF and HIF. It is necessary to note that all the battery parameters employed to estimate the SOC are identified based on the improved FF-RLS algorithm. First, the test battery is fully charged according to the CC-CV charging strategy. After rest for 2 hours, the current profiles acquired based on urban dynamometer driving schedule (UDDS) is repetitively implemented until the terminal voltage drops to the cut-off voltage, i.e., 2.75 V. All of the experiments are carried out at a room temperature of 25 °C. The reference initial SOC value is 100%, and to validate the independence of different methods on the initial value, the initial SOC is mistakenly set to 60%. The detailed comparison of different algorithms is illustrated in Fig. 5 and Table IV, respectively. It can be clearly found that EKF, HIF, AEKF and the proposed algorithm can all compensate the large error incurred by the preset differences. As listed in Table IV, the duration to reach the reference SOC value, which defined as the time when the estimate is stabilized within the 5% error bound, is respectively 45 s, 40 s, 46 s and 30 s, highlighting that the proposed algorithm responses faster than other algorithms. It can also be observed that the SOC estimation based on the AHIF attains least estimation error during the whole discharging process, and the maximum absolute error, mean absolute error and RMSE are 0.7%, 0.42%, and 0.6%, respectively. Obviously, the AHIF exhibits highest estimation accuracy among these four filters. The reason is that the AHIF does not assume that the statistical characteristics of noise are known in advance, that is imperative in Kalman filter [3], and instead suppresses the norm of interference into the designated range, thereby enabling the observer to solve the bounded signal and improving its robustness dramatically. In addition, the precise estimation supplies trustable fundamental knowledge for singularity analysis of SOC. If the maximum absolute error, mean absolute error and RMSE are less than 1%, the possibility of singularity occurrence can be almost avoided.

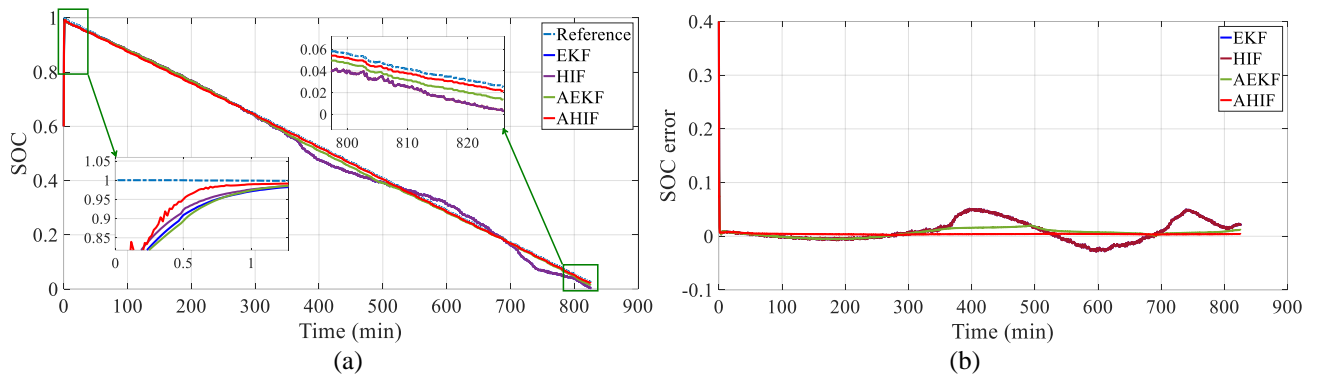


Fig. 5. Results of SOC estimation in case of different estimators: (a) referenced and estimated SOC and (b) corresponding error.

Table IV. Comparison results with different algorithms.

Algorithm	Convergence time (s)	Maximum absolute error (%)	Mean absolute error (%)	RMSE (%)
EKF	45	5.08	1.6	2.22
HIF	40	5.144	1.6	2.21
AEKF	46	2.014	0.79	1.05
AHIF	30	0.7	0.42	0.6

For the sake of further validating the performance of our proposed method, the SOC estimation errors based on different models are compared in Table V. Due to the same battery type and similar operational conditions, the results of the proposed method are compared with those of the electrochemical model referred from [31, 48], where they conduct the estimation based on the simplified electrochemical model and the ASR-SPKF and proportional-integral (PI) observer. The maximum absolute error and RMSE based on the reduced-order electrochemical model with the AEKF algorithm are respectively 5.6% and 2.57%, which are obviously larger than those of the proposed algorithm. In addition, the reduced-order electrochemical model is inferior to the proposed method in terms of the convergence time. As can be found, the shortest convergence time of the electrochemical model method is 123 s, whereas the proposed method requires only 30 s to converge to the reference value, and it is only about one-fourth of that of the reduced-order electrochemical model with the A-SPKF algorithm. To sum up, the comparison results manifest that the proposed method outperforms most of the electrochemical model-based reported in the literature.

Table V. Comparison of SOC estimation results based on different models.

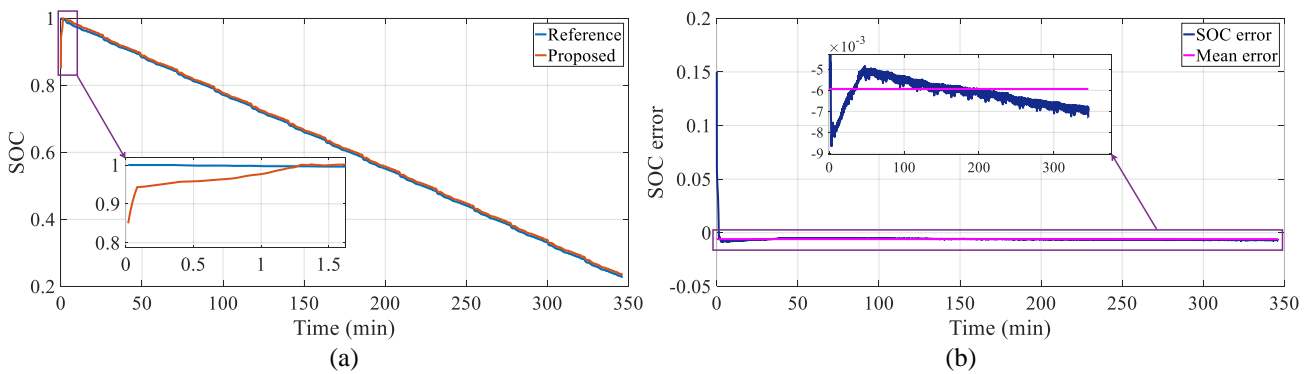
Model	Algorithm	Convergence time (s)	Maximum absolute error (%)	RMSE (%)
Proposed		30	0.7	0.6
Reduced-order electrochemical model [31]	AEKF	1116	5.6	2.57
	A-SPKF	123	3.1	1.68
	ASR-SPKF	129	3.1	1.68
Single particle model [48]	PI	/	3	1.2

C. SOC Estimation at Different Temperatures

All the above validations and comparisons are conducted at room temperature. It is vital to verify the thermal adaptability of the algorithm existing in practice. As described in Section II, the battery parameters change dramatically with operating temperature. Here, the performance of designed SOC estimation algorithm is further investigated under different operating conditions, such as constant low temperature ($-20\text{ }^{\circ}\text{C}$) and time-varying temperature conditions. In this discussion, the effects of inaccurate initial SOC is also considered to evaluate the convergence performance of proposed algorithm at different temperatures. The initial value is set to 85% when estimating the SOC, and obviously, the error is 15%.

1). SOC Estimation at Low Temperature

It is well acknowledged that battery capacity and output power degrade at low temperature. This may affect battery SOC estimation accuracy to a large extent. Similar as the experiment before, the UDDS current profile is still imposed at $-20\text{ }^{\circ}\text{C}$ after the battery is fully charged. Note that the cell is placed in the thermal controlled chamber for 3 hours until the experiment starts. Fig. 6 demonstrates the estimated SOC, estimated voltage and corresponding errors when compared with their reference values. The SOC estimation result and corresponding error are provided in Fig. 6 (a) and (b), respectively; in which we can find that the overall error is less than 1% except the initial setting difference. In addition, it is obviously found that the output voltage of model can track the measured value precisely, thus contributing to accurate estimation of SOC, and the mean absolute error is less than 0.014 V, only accounting for 0.38% of the nominal voltage. All the statistical comparisons at different temperatures are summarized in Table VI. We can find that the RMSE of SOC and voltage are 0.67% and 0.0198 V even at a low temperature, thereby manifesting capabilities of preferable SOC estimation and voltage tracking. In summary, the verification test proves that the proposed method can accurately estimate the SOC in a low temperature condition.



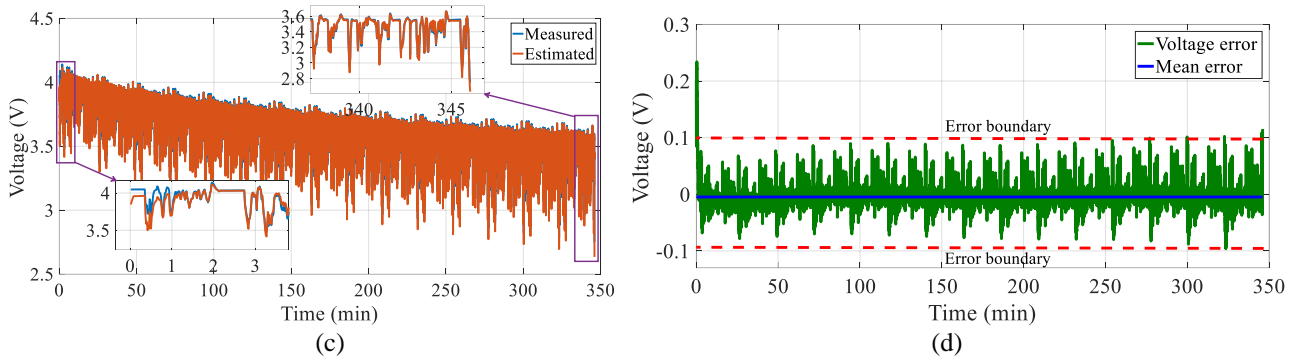


Fig. 6. The SOC validation results in case of $-20\text{ }^{\circ}\text{C}$: (a) the comparison results of the reference SOC and estimated SOC; (b) SOC estimation error; (c) the comparison results of the measured voltage and estimated voltage; (d) voltage estimation error.

2). Evaluation with Time-Varying Temperature

In practice, batteries are not easy to operate with constant temperature. To further validate the performance of proposed algorithm, the operating temperature continuously varies from $28\text{ }^{\circ}\text{C}$ to $7\text{ }^{\circ}\text{C}$. In the test, the battery is also charged by the CC-CV scheme, followed by a three hours' rest in the thermal controlled chamber of $28\text{ }^{\circ}\text{C}$. Then, the battery is discharged under the federal urban driving schedule (FUDS) cycle until the voltage decreases to 2.75 V . In the experiment, the battery temperature decreases from $28\text{ }^{\circ}\text{C}$ to $7\text{ }^{\circ}\text{C}$ by gradual cooling. Fig. 7 (a) depicts the temperature variation. The SOC estimation result and error are shown in Fig. 7 (b) and (c), where the GA-AHIF indicates the model parameters are identified by GA, and the SOC is estimated by the AHIF. It can be seen from Fig. 7 (b), both the GA-AHIF and proposed SOC estimation method can quickly offset the initial error and track the reference curve precisely. The convergence time, maximum absolute error, mean absolute error and RMSE of the proposed algorithm are 27 s, 0.79%, 0.24% and 0.42%, respectively. However, the convergence time of GA-AHIF based method is around four times longer than the proposed method. Besides, the GA-AHIF method incurs larger estimation error, which gradually increases to 2.68% in the end of the test. Fig. 7 (d) and (e) present the measured voltage, model output and errors. Similar as the SOC, the terminal voltage based on the proposed method is much smoother and more accurate than that of the GA-AHIF method, manifesting its strong adaptability to temperature variation. Thanks to the improved FF-RLS algorithm, the model parameters can be accurately adjusted online even in the case of low current excitation. The online identified OCV is shown in Fig. 7 (f). It is obvious that the OCV changes with temperature, and in other words, the necessity of updating OCV dynamically according to temperature variation is justified. The statistical comparisons at time-varying temperatures are listed in Table VI. It can be found that the maximum absolute error, mean absolute error and RMSE based on the GA-AHIF algorithm are 2.68%, 0.93% and 1.3%,

respectively. While the maximum absolute error of the proposed method is lower than 0.8%, less than one third of that by the GA-AHIF method. The mean absolute error and RMSE of the proposed method are lower than 0.3% and 0.5%, respectively, indicating that the preferable estimation performance can be achieved by the proposed fusion estimation method.

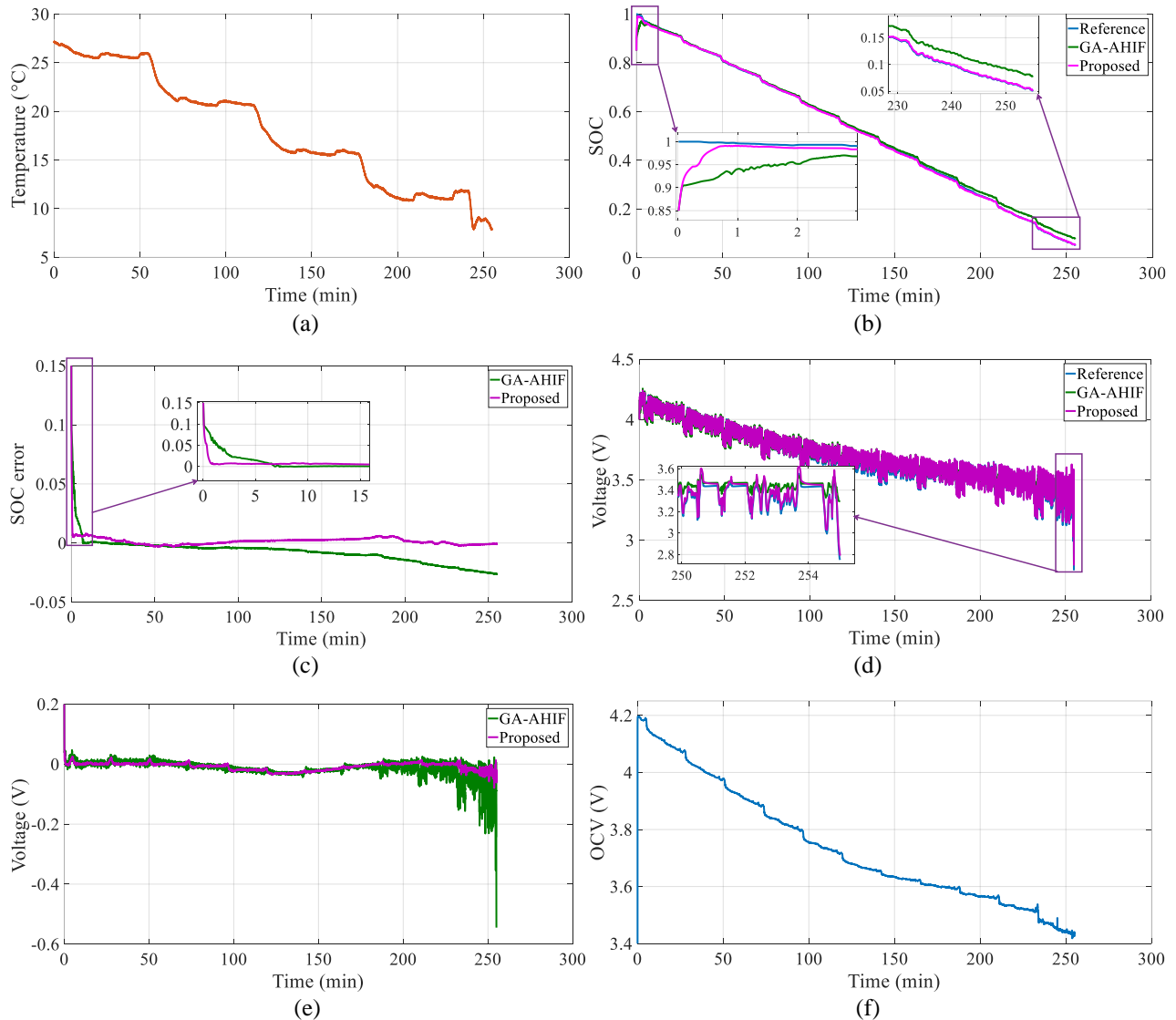


Fig. 7. Results of SOC estimation in case of time-varying temperature: (a) Temperature versus time; (b) SOC versus time; (c) SOC estimation error versus time; (d) OCV versus time; (e) Voltage estimation comparison result versus time; (f) Voltage estimation error versus time.

Table VI Statistical data of estimated SOC and voltage at different temperatures

Temperature	Method	SOC			Voltage			
		Convergence time (s)	Maximum absolute error (%)	Mean absolute error (%)	RMSE (%)	Maximum absolute error (V)	Mean absolute error (V)	RMSE (V)
Constant	Proposed	36	0.8	0.62	0.67	0.115	0.0132	0.0198
	Proposed	27	0.79	0.24	0.42	0.0795	0.0103	0.0148
Variable	GA-AHIF	129	2.68	0.93	1.3	0.545	0.0169	0.0284

D. SOC Estimation with Aged Cells

Based on the proposed fusion estimation method, the cells with different aging status are tested to validate the performance of proposed SOC estimation algorithm. After fully charged according to the CC-CV charging strategy, the test battery is cycled with UDDS current at room temperature until the terminal voltage drops to 2.75 V. By extracting the characteristic parameters of the charging process, the battery SOH is firstly estimated. When the battery is discharged, the updated capacity is imported to estimate the SOC. In this case, the initial SOC is set to 20% for all the aging cells, and obviously the difference is 80%. The SOC estimation results in terms of aging cells are illustrated in Fig. 8 and Table VII, respectively. Here, we only select four different aging status for discussion, i.e. 97% SOH, 93% SOH, 88% SOH and 85% SOH. As can be seen, with the aging of battery, the total discharging time decreases gradually in the same working conditions. The estimated SOC against different aging status can all converge to the referred values, proving the robustness and adaptivity of proposed algorithm when dealing with aged cells. The maximum estimation error of SOC with respect to four different SOH status locates within the same region which corresponds to the SOC range of 60% to 30%. This is because the SOC-OCV correlation is quite flat in this range, as depicted in Fig. 8 (c). The SOC estimation error based on the proposed method can be restricted within 1.2% under this case. The remaining battery parameters including OCV, ohmic resistance, polarization resistance and time constant are shown in Fig. 8 (c) to (f). We can find that only slight difference among different OCV curves exists when the battery ages. When SOC drops to 4% from 60%, the OCV decreases by 0.016 V, which may lead to the SOC estimation error of 1.4%. Nonetheless, the battery parameters change obviously under different aging conditions. From the perspective of the single cycle, the ohmic resistance in the middle SOC region is small and varies slowly, whereas the ohmic resistance in the lower SOC region increases quickly, and moreover the ohmic resistance corresponding to the lower SOC region is usually greater than that of higher SOC region. From the global perspective, the ohmic resistance tends to increase gradually with the decline of SOH. The similar variation trend also applies to the polarization resistance. Hence, we can conclude that real-time update of battery parameters responding to different aging status are imperative to improve the accuracy of SOC estimation. The comparison results clearly prove the effectiveness of proposed SOC estimation algorithm in a wide life cycle.

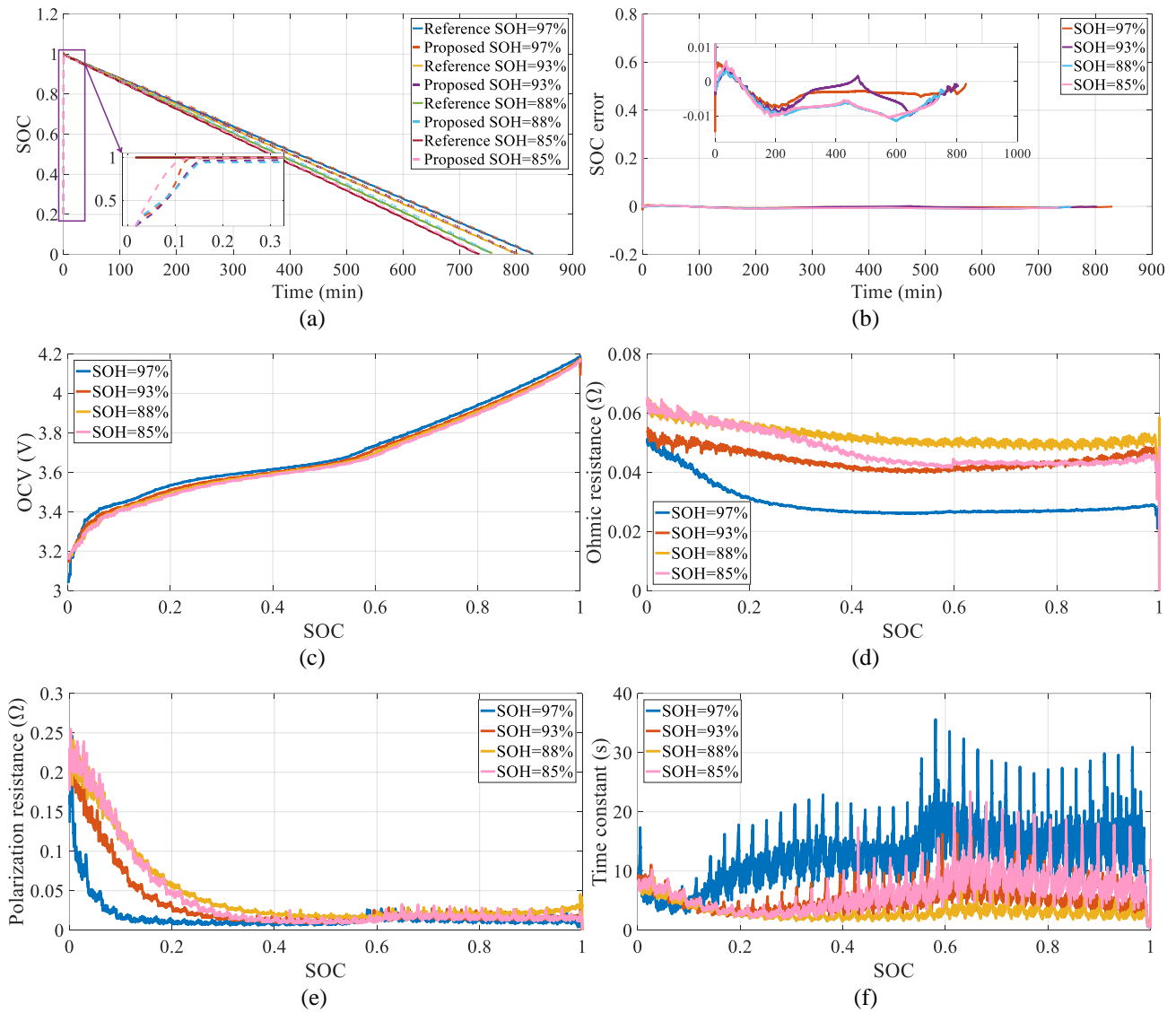


Fig. 8. Results of SOC estimation in case of aging cells: (a) reference and estimated SOC and (b) SOC error; (c) estimated OCV; (d) estimated ohmic resistance; (e) estimated polarization resistance; (f) estimated time constant.

Table VII Summarization of SOC and voltage estimation results with aging cell

SOH	SOC				Voltage		
	Convergence time (s)	Maximum absolute error (%)	Mean absolute error (%)	RMSE (%)	Maximum absolute error (V)	Mean absolute error (V)	RMSE (V)
97%	33	0.73	0.37	0.76	0.052	0.0082	0.013
93%	36	0.97	0.43	0.86	0.059	0.0082	0.0128
88%	57	1.16	0.7	1.02	0.067	0.0092	0.0142
85%	47	1.03	0.71	0.93	0.088	0.0094	0.0146

V. CONCLUSION

In this paper, an adaptive fusion algorithm is proposed to investigate the influence of battery degradation and dynamic working temperature on state of charge estimation of lithium-ion batteries. An improved online identification algorithm based on the improved recursive least square method with the forgetting factor is applied to identify model parameters over a wide temperature range of $-20\text{ }^{\circ}\text{C}$ to $50\text{ }^{\circ}\text{C}$. The least square support vector machine algorithm is employed to conduct the accurate state of health estimation, which in turn

contributes to estimation of battery state of charge. The experimental results reveal that the state of health estimation error is less than 2%. The adaptive H-infinity filter is proposed to estimate the state of charge based on the dynamically updated state of health and precise battery model. By comparing with the commonly used extended Kalman filter, adaptive extended Kalman filter and H-infinity filter algorithms, the proposed algorithm exhibits higher estimation accuracy, fast convergence speed and better adaptation to variation of external operating temperatures and battery degradation. The comprehensive evaluation of algorithm highlights its broad application potential in joint estimation of state of charge and state of health for lithium-ion batteries. In addition, the proposed method can bring significant reference to singularity prediction of the state of charge. When the battery management system obtains more accurate state of charge estimation, the threshold for the residual of state of charge can be further reduced to avoid misjudgment when performing the singularity prediction.

In the future, more in-depth analysis in terms of the relationship between state of charge estimation and its singularity prediction will be conducted. Moreover, we will program the algorithm in the control unit of the printed circuit board and validate the estimation performance of designed battery management system in actual battery packs of electric vehicles. In particular, when inconsistency of temperature and capacity exists among cells in the pack, how to deal with the imbalance and supply the authoritative estimation needs to be further investigated.

ACKNOWLEDGEMENTS

This work was supported in part by the National Natural Science Foundation (No. 51775063 and No. 61763021), in part by the National Key R&D Program of China (No. 2018YFB0104000), in part by the Fundamental Research Funds for the Central Universities (No. 2018CDQYQC0035), and in part by the EU-funded Marie Skłodowska-Curie Individual Fellowships Project under Grant 845102-HOEMEV-H2020-MSCA-IF-2018.

REFERENCES

- [1] C. Zhang, F. Yang, X. Ke, Z. Liu, and C. Yuan, "Predictive modeling of energy consumption and greenhouse gas emissions from autonomous electric vehicle operations," *Applied Energy*, vol. 254, p. 113597, 2019.
- [2] Y. Liu, J. Li, Z. Chen, D. Qin, and Y. Zhang, "Research on a multi-objective hierarchical prediction energy management strategy for range extended fuel cell vehicles," *Journal of Power Sources*, vol. 429, pp. 55-66, 2019.

- [3] P. Shrivastava, T.K. Soon, M.Y.I.B. Idris, and S. Mekhilef, "Overview of model-based online state-of-charge estimation using Kalman filter family for lithium-ion batteries," *Renewable and Sustainable Energy Reviews*, vol. 113, p. 109233, 2019.
- [4] X. Li, L. Zhang, Z. Wang, and P. Dong, "Remaining useful life prediction for lithium-ion batteries based on a hybrid model combining the long short-term memory and Elman neural networks," *Journal of Energy Storage*, vol. 21, pp. 510-518, 2019.
- [5] K. Liu, K. Li, Q. Peng, and C. Zhang, "A brief review on key technologies in the battery management system of electric vehicles," *Frontiers of Mechanical Engineering*, vol. 14, pp. 47-64, 2019.
- [6] H. Rahimi-Eichi, U. Ojha, F. Baronti, and M. Chow, "Battery Management System: An Overview of Its Application in the Smart Grid and Electric Vehicles," *IEEE Industrial Electronics Magazine*, vol. 7, pp. 4-16, 2013.
- [7] C. Chen, R. Xiong, R. Yang, W. Shen, and F. Sun, "State-of-charge estimation of lithium-ion battery using an improved neural network model and extended Kalman filter," *Journal of Cleaner Production*, vol. 234, pp. 1153-1164, 2019.
- [8] X. Li, Z. Wang, and J. Yan, "Prognostic health condition for lithium battery using the partial incremental capacity and Gaussian process regression," *Journal of Power Sources*, vol. 421, pp. 56-67, 2019.
- [9] Z. Chen, Q. Xue, R. Xiao, Y. Liu, and J. Shen, "State of Health Estimation for Lithium-ion Batteries Based on Fusion of Autoregressive Moving Average Model and Elman Neural Network," *IEEE Access*, vol. 7, pp. 102662-102678, 2019.
- [10] T. Feng, L. Yang, X. Zhao, H. Zhang, and J. Qiang, "Online identification of lithium-ion battery parameters based on an improved equivalent-circuit model and its implementation on battery state-of-power prediction," *Journal of Power Sources*, vol. 281, pp. 192-203, 2015.
- [11] X. Li, Z. Wang, L. Zhang, C. Zou, and D.D. Dorrell, "State-of-health estimation for Li-ion batteries by combing the incremental capacity analysis method with grey relational analysis," *Journal of Power Sources*, vol. 410-411, pp. 106-114, 2019.
- [12] F. Guo, G. Hu, and R. Hong, "A parameter adaptive method with dead zone for state of charge and parameter estimation of lithium-ion batteries," *Journal of Power Sources*, vol. 402, pp. 174-182, 2018.
- [13] S.-C. Huang, K.-H. Tseng, J.-W. Liang, C.-L. Chang, and G.M. Pecht, "An Online SOC and SOH Estimation Model for Lithium-Ion Batteries," *Energies*, vol. 10, 2017.
- [14] F. Yang, X. Song, F. Xu, and K. Tsui, "State-of-Charge Estimation of Lithium-Ion Batteries via Long Short-Term Memory Network," *IEEE Access*, vol. 7, pp. 53792-53799, 2019.
- [15] S. Nejad, D.T. Gladwin, and D.A. Stone, "A systematic review of lumped-parameter equivalent circuit models for real-time estimation of lithium-ion battery states," *Journal of Power Sources*, vol. 316, pp. 183-196, 2016.
- [16] X. Lai, Y. Zheng, and T. Sun, "A comparative study of different equivalent circuit models for estimating state-of-charge of lithium-ion batteries," *Electrochimica Acta*, vol. 259, pp. 566-577, 2018.
- [17] R. Xiong, L. Li, Z. Li, Q. Yu, and H. Mu, "An electrochemical model based degradation state identification method of Lithium-ion battery for all-climate electric vehicles application," *Applied Energy*, vol. 219, pp. 264-275, 2018.
- [18] A. Jokar, B. Rajabloo, M. Désilets, and M. Lacroix, "Review of simplified Pseudo-two-Dimensional models of lithium-ion batteries," *Journal of Power Sources*, vol. 327, pp. 44-55, 2016.
- [19] M. Ye, H. Guo, and B. Cao, "A model-based adaptive state of charge estimator for a lithium-ion battery using an improved adaptive particle filter," *Applied Energy*, vol. 190, pp. 740-748, 2017.
- [20] G.L. Plett, "Extended Kalman filtering for battery management systems of LiPB-based HEV battery packs: Part 3. State and parameter estimation," *Journal of Power Sources*, vol. 134, pp. 277-292, 2004.
- [21] Z. Chen, X. Li, J. Shen, W. Yan, and R. Xiao, "A Novel State of Charge Estimation Algorithm for Lithium-Ion Battery Packs of Electric Vehicles," *Energies*, vol. 9, 2016.

- [22] J. Peng, J. Luo, H. He, and B. Lu, "An improved state of charge estimation method based on cubature Kalman filter for lithium-ion batteries," *Applied Energy*, vol. 253, p. 113520, 2019.
- [23] C. Huang, Z. Wang, Z. Zhao, L. Wang, C.S. Lai, and D. Wang, "Robustness Evaluation of Extended and Unscented Kalman Filter for Battery State of Charge Estimation," *IEEE Access*, vol. 6, pp. 27617-27628, 2018.
- [24] M. Gholizadeh and A. Yazdizadeh. (2019), State of charge estimation of a lithium-ion battery using robust non-linear observer approach. *IET Electrical Systems in Transportation* 9(1), 1-7. Available: <https://digital-library.theiet.org/content/journals/10.1049/iet-est.2018.0002>
- [25] C. Chen, R. Xiong, and W. Shen, "A lithium-ion battery-in-the-loop approach to test and validate multiscale dual H infinity filters for state-of-charge and capacity estimation," *IEEE Transactions on power Electronics*, vol. 33, pp. 332-342, 2017.
- [26] Z. Wei, J. Zhao, C. Zou, T.M. Lim, and K.J. Tseng, "Comparative study of methods for integrated model identification and state of charge estimation of lithium-ion battery," *Journal of Power Sources*, vol. 402, pp. 189-197, 2018.
- [27] X. Hu, S. Li, H. Peng, "A Comparative Study of Equivalent Circuit Models for Li-Ion Batteries," *Journal of Power Sources*, vol. 198, pp. 359-367, 2012.
- [28] J. Yang, B. Xia, Y. Shang, W. Huang, and C.C. Mi, "Adaptive State-of-Charge Estimation Based on a Split Battery Model for Electric Vehicle Applications," *IEEE Transactions on Vehicular Technology*, vol. 66, pp. 10889-10898, 2017.
- [29] X. Han, M. Ouyang, L. Lu, J. Li, "Simplification of physics-based electrochemical model for lithium ion battery on electric vehicle. Part I: diffusion simplification and single particle model," *Journal of Power Sources*, vol. 278, pp. 802-813, 2015.
- [30] H. Li, W. Zhang, X. Yang, H. Jiang, Y. Wang, T. Yang, L. Chen, H. Shen, "State of charge estimation for lithium-ion battery using an electrochemical model based on electrical double layer effect." *Electrochimica Acta*, vol. 326, p. 134966, 2019.
- [31] Y. Bi and S.-Y. Choe, "An adaptive sigma-point Kalman filter with state equality constraints for online state-of-charge estimation of a Li (NiMnCo) O₂/Carbon battery using a reduced-order electrochemical model," *Applied Energy*, vol. 258, p. 113925, 2020.
- [32] K. Lee, M. Dai, and C. Chuang, "Temperature-Compensated Model for Lithium-Ion Polymer Batteries With Extended Kalman Filter State-of-Charge Estimation for an Implantable Charger," *IEEE Transactions on Industrial Electronics*, vol. 65, pp. 589-596, 2018.
- [33] L. Zheng, J. Zhu, D.D.-C. Lu, G. Wang, and T. He, "Incremental capacity analysis and differential voltage analysis based state of charge and capacity estimation for lithium-ion batteries," *Energy*, vol. 150, pp. 759-769, 2018.
- [34] X. Li, Z. Wang, and L. Zhang, "Co-estimation of capacity and state-of-charge for lithium-ion batteries in electric vehicles," *Energy*, vol. 174, pp. 33-44, 2019.
- [35] X. Wu, X. Li, and J. Du, "State of Charge Estimation of Lithium-Ion Batteries Over Wide Temperature Range Using Unscented Kalman Filter," *IEEE Access*, vol. 6, pp. 41993-42003, 2018.
- [36] Q. Song, Y. Mi, and W. Lai, "A Novel Variable Forgetting Factor Recursive Least Square Algorithm to Improve the Anti-Interference Ability of Battery Model Parameters Identification," *IEEE Access*, vol. 7, pp. 61548-61557, 2019.
- [37] R. Xiong, F. Sun, H. He, and T.D. Nguyen, "A data-driven adaptive state of charge and power capability joint estimator of lithium-ion polymer battery used in electric vehicles," *Energy*, vol. 63, pp. 295-308, 2013.
- [38] Z. Wei, C. Zou, F. Leng, B.H. Soong, and K. Tseng, "Online Model Identification and State-of-Charge Estimate for Lithium-Ion Battery With a Recursive Total Least Squares-Based Observer," *IEEE Transactions on Industrial Electronics*, vol. 65, pp. 1336-1346, 2018.
- [39] Z. Chen, C.C. Mi, Y. Fu, J. Xu, and X. Gong, "Online battery state of health estimation based on Genetic Algorithm for electric and hybrid vehicle applications," *Journal of Power Sources*, vol. 240, pp. 184-192, 2013.

- [40] Z. Chen, X. Shu, M. Sun, J. Shen, and R. Xiao, "Charging strategy design of lithium-ion batteries for energy loss minimization based on minimum principle," in *2017 IEEE Transportation Electrification Conference and Expo, Asia-Pacific (ITEC Asia-Pacific)*, 2017, pp. 1-6, 2017.
- [41] Z. Chen, X. Shu, R. Xiao, W. Yan, Y. Liu, and J. Shen, "Optimal charging strategy design for lithium-ion batteries considering minimization of temperature rise and energy loss," *International Journal of Energy Research*, vol. 43, pp. 4344-4358, 2019.
- [42] D. Yang, Y. Wang, R. Pan, R. Chen, and Z. Chen, "State-of-health estimation for the lithium-ion battery based on support vector regression," *Applied Energy*, vol. 227, pp. 273-283, 2018.
- [43] Z. Chen, M. Sun, X. Shu, R. Xiao, and J. Shen, "Online State of Health Estimation for Lithium-Ion Batteries Based on Support Vector Machine," *Applied Sciences*, vol. 8, p. 925, 2018.
- [44] Z. Chen, X. Xia, M. Sun, J. Shen, and R. Xiao, "State of Health Estimation of Lithium-Ion Batteries Based on Fixed Size LS-SVM," in *2018 IEEE Vehicle Power and Propulsion Conference (VPPC)*, 2018, pp. 1-6, 2018.
- [45] W. An-na, Z. Yue, H. Yun-tao, and L.I. Yun-lu, "A novel construction of SVM compound kernel function," in *2010 International Conference on Logistics Systems and Intelligent Management (ICLSIM)*, 2010, pp. 1462-1465, 2010.
- [46] Y. Deng, H. Ying, J. E, H. Zhu, K. Wei, J. Chen, F. Zhang, and G. Liao, "Feature parameter extraction and intelligent estimation of the State-of-Health of lithium-ion batteries," *Energy*, vol. 176, pp. 91-102, 2019.
- [47] A. Eddahech, O. Briat, and J.-M. Vinassa, "Determination of lithium-ion battery state-of-health based on constant-voltage charge phase," *Journal of Power Sources*, vol. 258, pp. 218-227, 2014.
- [48] L. Zheng, L. Zhang, J. Zhu, G. Wang, and J. Jiang, "Co-estimation of state-of-charge, capacity and resistance for lithium-ion batteries based on a high-fidelity electrochemical model," *Applied Energy*, vol. 180, pp. 424-434, 2016.